

Analysis of a permanent magnet synchronous machine used in hazardous locations

Nijan Yogal¹, Christian Lehrmann¹

¹ Physikalisch-Technische Bundesanstalt, Fachbereich 3.63 „Explosionengeschützte elektrische Antriebssysteme“, Braunschweig

The use of a permanent magnet synchronous machines (PMSMs) to achieve high performance and high energy efficiency in modern industrial technology has increased rapidly in recent decades. Similarly, the demand for PMSMs in hazardous locations has been increasing as well. This work focuses on the safe operation of PMSMs in hazardous locations, as it undergoes through a series of mechanical, electrical and thermal tests. These tests methods ensure that no hot surfaces, electrical arcs or sparks occur during normal or possible failure operation. In addition, it ensures that there are no possible failure conditions in all inner and outer parts of the PMSMs that can lead to high energy which may be responsible for ignition. The PMSM installed in hazardous areas need to have protection against the possibility of ignition. Therefore, the thermal protection of the PMSM using PTC thermistors sensors are tested so that the PMSM stops operating in case of higher thermal heating of stator winding. Different influencing input quantities from the instruments used for measurement in the test bench are studied and the uncertainty is analysed. While determining the efficiency of the machines the final measurement uncertainty of the test bench is examined and presented with "Guide to the Expression of Uncertainty in Measurement" (GUM) procedure. Besides the testing of the PMSM, this work, therefore, deals mainly with problems concerning the demagnetization of the PM during abnormal operating condition of PMSM using FEM simulation.

1 Introduction

The safety, the secure operation and the design of electrical machines in hazardous environments are defined according to international and regional standards [1] and [2]. Electrical machines with the "Increased Safety" ignition protection classification (abbreviated as "Ex e") [3] are manufactured for safe operation and should be mechanically and electrically tested so that no hot surfaces, electrical arcs or sparks occur during normal operation. There should also be no possible failure conditions in all inner and outer parts of the machines. The potential sources of ignition that may occur in permanent magnet synchronous machines (PMSMs) during operation are hot surfaces, electrical discharges, and mechanically generated sparks. It is important and necessary that there should not be enough energy in the electrical machines for ignitions. Till now, there has been no proper method of type testing PMSMs which need to be able to operate while remaining flameproof in high-risk hazardous environments. This paper addresses the mechanical, electrical and thermal tests that are required for PMSMs to operate safely.

2 Study of magnetic material properties used for manufacturing rotor and stator of PMSM

In manufacturing explosion-protected machines, special attention must be paid to the materials that are used in the manufacturing process. Materials should be used which have already proved to have satisfactory characteristics (behaviour) in normal operation and also in the defined temperature class operation.

Therefore, the magnetic properties of NO electrical sheets that are used for manufacturing the stators and rotors core of PMSMs are studied at a higher temperature and frequency which is

presented in paper [4]. Similarly, the magnetic properties of the permanent magnet that are used in the rotors of the test PMSMs are also studied and presented in paper [5].

2.1 Ring core measurement of non-oriented electrical steel sheets of PMSM

The iron core of the electrical machines is made of non-oriented (NO) electrical sheets. It provides the path for the magnetic flux density. The operation of electrical machines heavily dependent on the maximum magnetic flux density that can occur in the iron core without the saturation resulting hotspot in iron. Due to iron core saturation the air gap flux density cannot be raised above 1 T, as in the stator slot teeth of electrical machines cause of flux fringing, the flux density is increased by factor 2, already about 2 T flux density [6], which is above the saturation limit (about 1.7-1.8 T). Therefore, NO electrical steel sheets of PMSM must be studied to avoid extensive saturation.

2.1.1. Measurement principles and measurement setup

The conceptual sketch [7] of measurement system for the ring test specimen of NO electrical steel sheet materials is carried out using standard IEC 60404-6 [8] and shown in Fig. 2.1 (a). The sinusoidal amplified signal is used as the source to excite the primary winding of the ring specimen measurement set-up. The function generator (TTi TGA1244) can vary the frequency for the test set-up in kHz range. The low power generated sinusoidal signal is amplified by a ratio of 1:100 via a power amplifier (Rohrer PA 2016). The measuring current transformer (Bergoz CT D0.05-B) is used to measure the primary exciting current and the differential probe (TESTEC TT SI9010A) is used to measure induced voltage in the secondary winding. The digital oscilloscope (Yokogawa DL6154) is used to monitor the primary exciting current and the secondary induced voltage simultaneously. Both the the primary exciting current and the secondary induced voltage are the important parameter to study the magnetic properties of non-oriented (NO) electrical sheets.

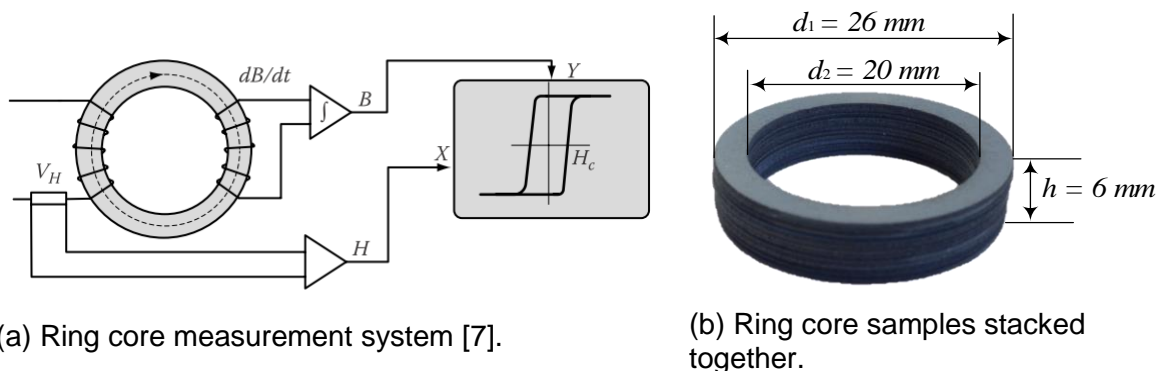


Fig. 2.1. Schematic representation of ring core measurement system with BH loop and ring core samples.

The magnetic field intensity H in the ring core is determined according to Ampers's law from the measured excitation primary winding current I_1 , the effective length of the magnetic path in the ring core sample l_e and the number of turns of the primary (excitation) winding N_1 :

$$\oint \vec{H} ds = N_1 I_1 = \Theta \quad (2.1)$$

A simplified form of equation (2.1) is:

$$H(l_e) = \frac{N_1 I_1}{l_e} \quad (2.2)$$

The magnetic flux density $B(t)$ is measured using the magnetic flux $\Phi(t)$ inside the core and the time variation of the flux results in induced voltage U_2 in the secondary coil with N_2 numbers of turns. According to Faraday's law:

$$B(t) = \frac{\phi(t)}{A_e} \quad (2.3)$$

$$\int_{t_0}^t U_2 dt = \Psi = N_2 \phi(t) \quad (2.4)$$

Using equation (2.3) and (2.4) gives:

$$B(t) = \frac{\int_{t_0}^t U_2 dt}{N_2 A_e} \quad (2.5)$$

The effective iron losses of the NO electrical sheets material (iron core) are calculated as IEC 60404-6:

$$P_{fe} = \frac{1}{T \cdot \rho_{Fe} \cdot V_e} \cdot \frac{N_1}{N_2} \int_0^T I_1(t) \cdot U_2(t) dt \quad (2.6)$$

Where T is the length of the magnetization period, ρ_{Fe} is the specific mass density of the test iron core material and V_e is the effective volume of the test specimen. In the ring core experimental setup, the voltages of the secondary winding: $U_2(t)$ are measured with different excitation of primary current $I_1(t)$. The specific iron losses P_{fe} , the magnetic flux density B and the form factor F are calculated with the measured primary current and the secondary voltage.

The BH loop measurement at 1.5 T magnetic flux density with varying frequencies is shown in Fig. 2.2 (a). Higher the frequencies, greater will be the loop area which results in higher hysteresis loss resulting in higher specific iron losses as depicted in Fig. 2.2 (b). In the experimental measurement, it is challenging to achieve the higher magnetic flux density at higher excitation frequencies.

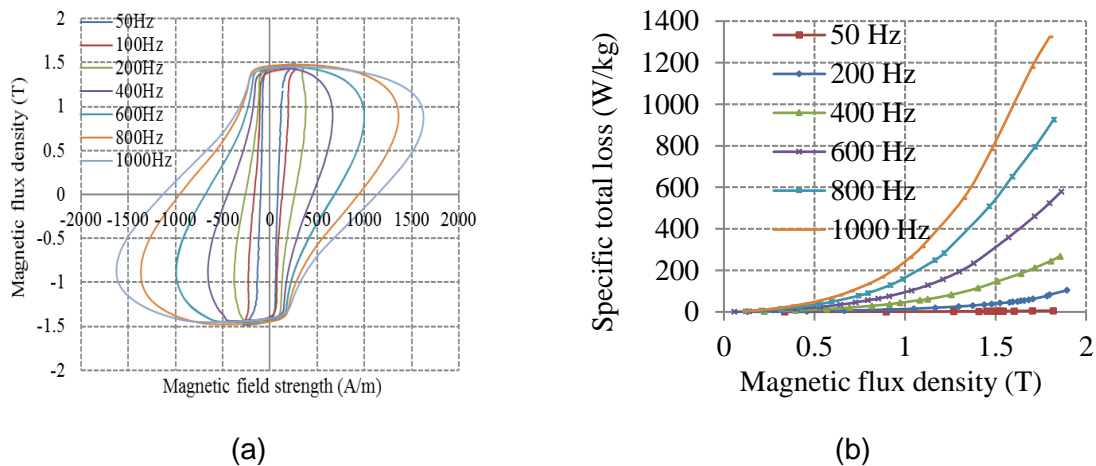
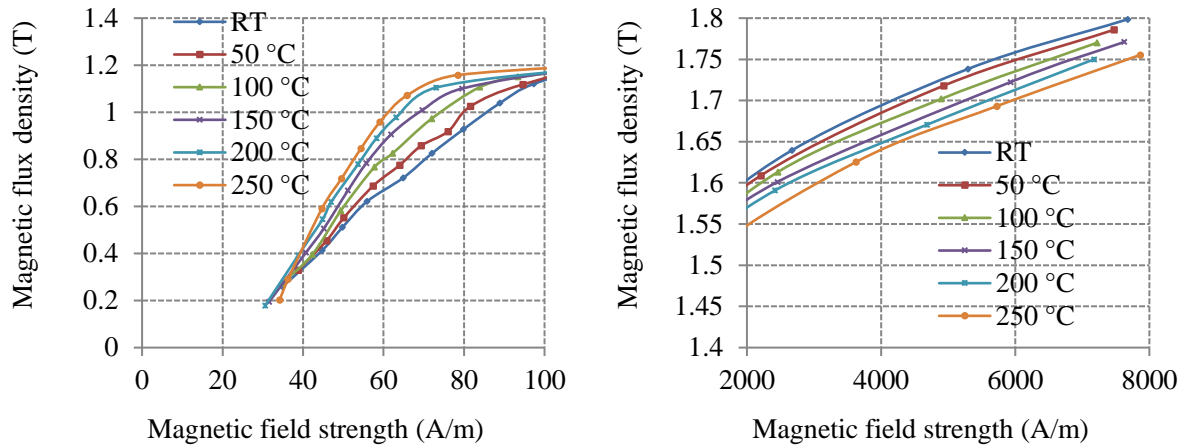


Fig. 2.2.: BH loop and the specific iron losses with different frequency for M450P-50K.

2.1.2. Effect of higher temperatures and frequencies in ring core measurement

The BH loop, BH curve due to change in temperature for M450P-50K is shown in Fig. 2.3. The temperature is varied from room temperature (RT) to 250 °C. As shown in Fig. 2.3 (a), at lower magnetic field strength, the magnetic flux density increases with increasing temperature. In comparison, the magnetic flux density decreases with increasing temperature at high magnetic field strength, as shown in Fig. 2.3 (b).

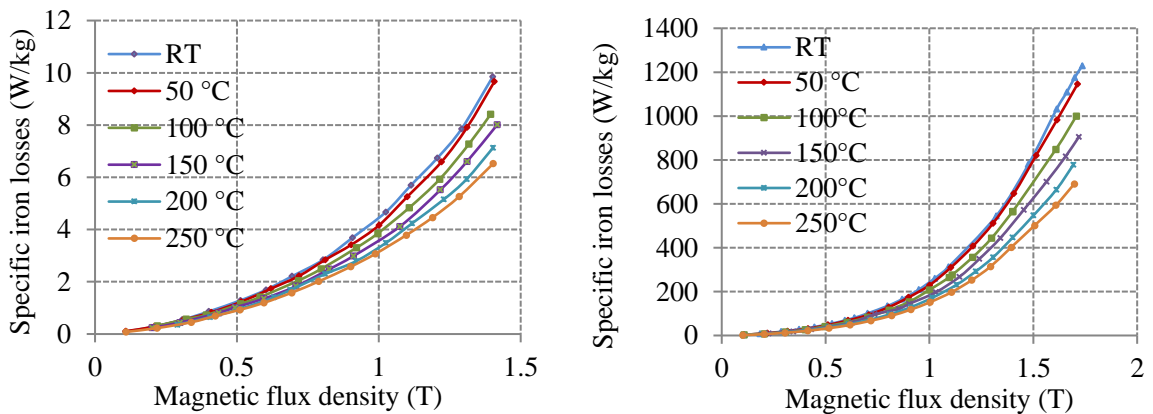


(a) *BH* curve at low magnetic field strength. (b) *BH* curve at high magnetic field strength.

Fig. 2.3. *BH* loop and *BH* curve for different temperature at 50 Hz.

The possible reason for higher B field with lower H field at higher temperature is that the orientation of the magnetic elements could be easier at high temperature. Therefore, several magnetic elements are oriented easily and faster and thereby the flux density is increased. But this phenomenon is dependent on the type of material and percentage of silicon content in manufacturing NO electrical sheets materials. In contrast, the ferromagnetic properties of materials disappeared at high temperature.

The specific iron losses decrease with increasing temperatures at both frequencies as shown in Fig. 2.4. The reason for this is the reduction of the eddy current losses at high temperature. The temporal change in the magnetic flux density causes an induced voltage. When an induced voltage is applied in an electrically conductive material, eddy current losses occur. As the temperature increases, the resistivity of the iron sheets is increased. If the sheet thickness remains constant, the resistance R increases with increase in temperature. Consequently, the eddy current losses are low at lower temperature.



(a) The specific iron losses at 100 Hz.

(b) The specific iron losses at 1000 Hz.

Fig. 2.4. The specific iron losses for different temperature and frequency.

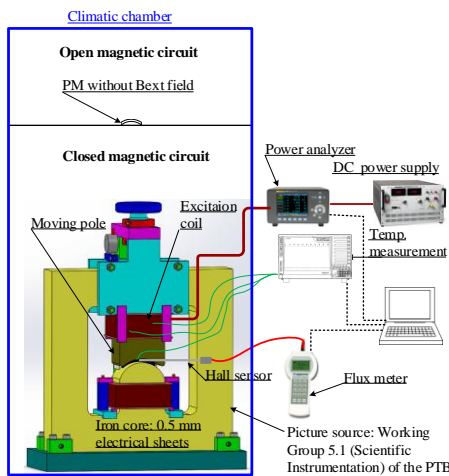
2.2 Demagnetization study of PM of PMSM

In general, inverter current limit must be below the critical motor current which would cause irreversible demagnetization of the hot rotor magnets (typically at 150 °C). Therefore, the study of irreversible demagnetization of the PM with respect to higher current and temperature

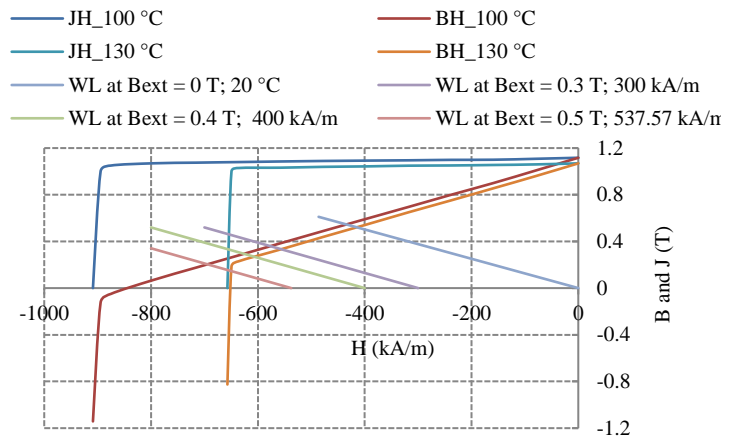
are of great interest for PMSM designers and manufacture. In explosive environments, the high surface temperature of PMSMs, due to the irreversible demagnetization of permanent magnets (PMs), could be a source of ignition leading to explosions. Numerous methods for analytical calculations along with finite element methods (FEMs) of magnetic loss and demagnetization in the PM have been presented [14], [13], [52], [16] and [53]. However, only little research work on measurement methods are available [53]. Therefore, in upcoming sections, the measurement method for demagnetization of a PM and the magnetic loss in the PM of a PMSM is presented.

The measurement setup for demagnetization of the PM with respect to external magnetic field and temperature is shown in Fig. 2.5. The closed magnetic circuit is similar to PMSM which comprises a magnetic circuit made of soft magnetic material such (NO electrical sheets) to guide the flux, an air gap and the permanent magnet (hard magnetic materials). When PMSM is in operation, then the PM is under demagnetization stress as a function of PM materials, geometry of magnet and temperature in the magnetic circuit. Therefore, in this section the demagnetization of the NdFeB permanent magnet as a function of external magnetic field and temperature is investigated.

The PM is exposed to a climatic chamber without and with an external magnetic field known as an open and a closed magnetic circuit, respectively. The climatic chamber was separated into two sections as shown in Fig. 2.5. In the upper section there is a PM in an open magnetic circuit, i.e. only a magnet without any external magnetic field. The lower section of the climatic chamber consists of a PM in a closed magnetic circuit with a DC external magnetic field. The PM was exposed to the external magnetic field with $B_{ext} = 0.3$ T, 0.4 T and 0.5 T. The external magnetic field B_{ext} is the field which is opposite to the PM self-magnetic field B_{pm} . However, the temperature of the climatic chamber was only set to 130 °C for all external field. In this section, the effect of the demagnetization of the PM with varying external negative magnetic field intensity with temperature are studied and presented.



(a) Pictorial representation of demagnetization measurement setup for PM [5].

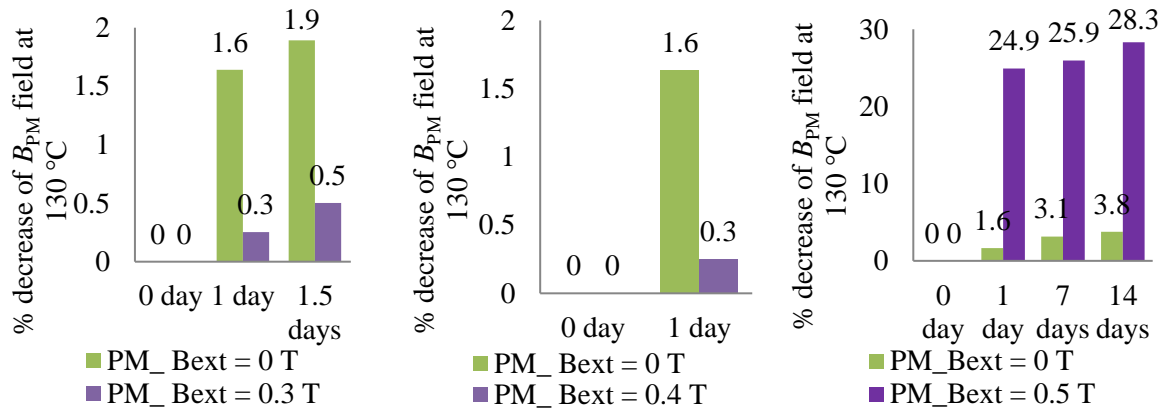


(b) A hysteresis curves of a PM material with working line (WL).

Fig. 2.5. Demagnetization measurement setup for PM with and without external magnetic field at higher temperature of 130 °C (a) and a hysteresis curves of a PM material (b).

The magnetic flux density B_{pm} of the PM samples were measured before storage and after exposure to the higher temperature and external magnetic field. The time-dependent demagnetization is seen as severe in the closed magnetic circuit with the external magnetic field compared to the open magnetic circuit without the external magnetic field as shown in Fig. 2.6. A lower external negative magnetic field intensity moves the WL or working point away (toward right) from the knee point and above the knee of the demagnetization curve. So, it is expected that the PM in the closed magnetic circuit should not be irreversibly demagnetized.

This phenomenon could be seen clearly in Fig. 2.6. (a) for 0.3 T (i.e. 300 kA/m) and in Fig. 2.6. (b) for 0.4 T (i.e. 400 kA/m) respectively. However, with the external magnetic field $B_{ext} = 0.5$ T (i.e. 537.57 kA/m) severe demagnetization of the PM occurs. This is because, the working line (WL) for 500 kA/m moves beyond and below the knee of the demagnetization curve. This is therefore the main reason why, in Fig. 2.6, the irreversible demagnetization of the PM in the closed magnetic circuit is higher compared to the open magnetic circuit after 1 day, 7 days and 14 days



(a) External magnetic field intensity of 300 kA/m induces 0.3 T flux density.

(b) External magnetic field intensity of 400 kA/m induces 0.4 T flux density.

(c) External magnetic field intensity of 537.57 kA/m induces 0.5 T flux density.

Fig. 2.6.: Percentage demagnetization of the PM at 130 °C with external magnetic field intensity of 300 kA/m (a), 400 kA/m (b) and 500 kA/m (c).

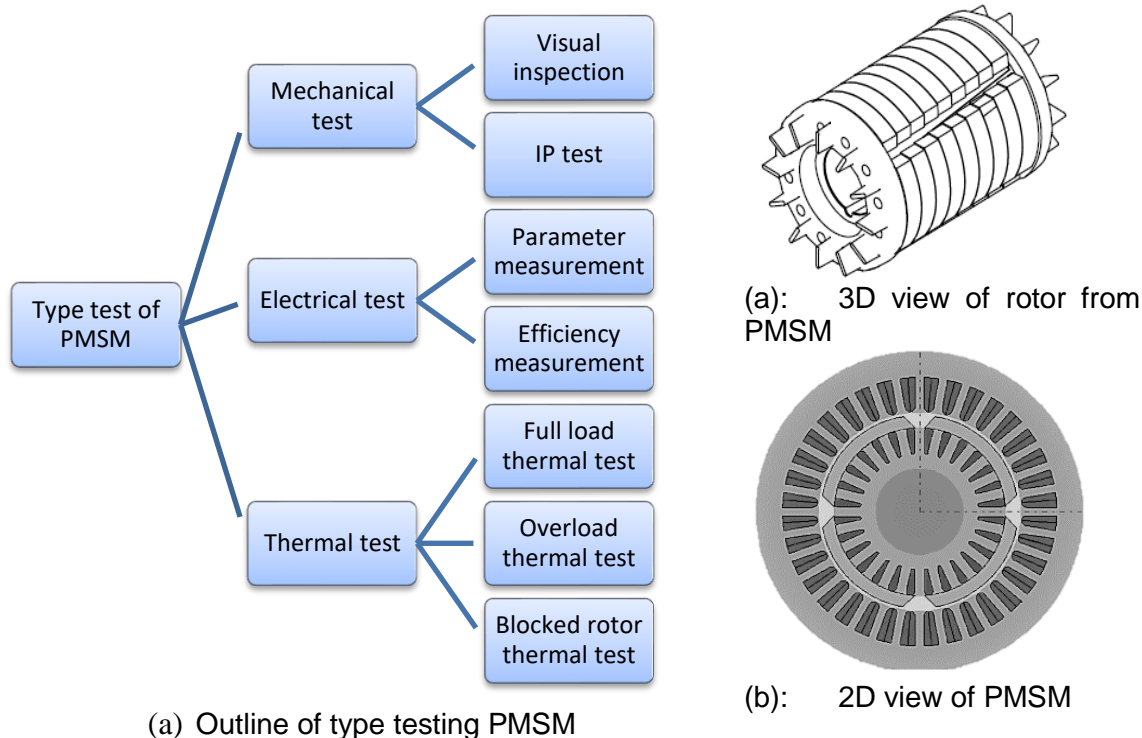
The designer of PMSM should properly calculate the negative field that the PM may be facing during the operation. The demagnetization of PM in closed magnetic circuit is a close representation of the permanent magnet motor or generator which illustrates what happens when the machines are operated in higher negative magnetic field intensity. It has been demonstrated with the help of a closed-circuit measurement with external magnetic field.

The results obtained indicate that the PM is completely demagnetized when it is operated below the knee point at 130 °C as shown in Fig. 2.6. (c). In conclusion, the study proves that the negative magnetic field forces the PM to work below the knee point which is not healthy for PMSM. Taken together, these results suggest that the PMSM must be designed in such a way that the PM always works above the knee point of demagnetization curve of the PM in the respective operating temperature.

3 Assessment and evaluation to develop type test and certification concept of PMSM

Current standards IEC 60079-0 [2] and IEC 60079-7 [3] on testing and certification of electrical machines mainly focused on asynchronous machines with “Ex eb” ignition protection classification. Even though the detail test method and certification concept for inverter fed squirrel cage induction machines with type of protection “Ex-eb” have been improved and presented in [9], however the study [9] does not take into account the test method and certification concept for inverter fed PMSM. Different types of PM motors for operation in hazardous locations are studied in [10]. However, the paper [10] only analyses and compares various aspects (rotor construction, working voltage, operating temperature, Stall/Start/Overload, etc.) of PMSM on the basis of existing standards but failed to present the analysis and validation with experimental measurement results. Nevertheless, there are still some interesting and relevant problems to be addressed while testing the inverter fed PMSM. None of the work till date focuses on test method and certification concept for inverter fed

PMSM. In this section, improved test methods are suggested for VSD fed PMSM. The focus on the measurement is on surface mounted permanent magnet synchronous machines (SPMSM), but it is also possible to conduct tests on interior mounted permanent magnet synchronous machines (IPMSM). The Fig. 3.1 shows the major issues concerning the mechanical, electrical and thermal tests that are required for PMSM (Fig. 3.1 (a) and (b)) with converter to operate safely in hazardous areas.



(a) Outline of type testing PMSM

Fig. 3.1.: Outline of type test focusing on protection of PMSM (b and c) in hazardous areas.

3.1 Mechanical testing of PMSM

The mechanical testing is performed by visual inspecting different parts of PMSM and monitoring protection provided by enclosures. The PMSM specimens need to be confirmed of its mechanical properties visually inspecting the constructional or dimensional requirements according to the international standards for specified rated PMSM. The standard IEC 60079-0 and increased safety “e” (EN 60079-7) in detail provide the general test of mechanical design of all electrical machines.

3.2 Electrical parameters of PMSM used for configuration of VSDs

The simple test methods is performed to measure and validate the most basic but important parameters such as resistance R_s , inductance l (l_d , l_q) and back-EMF voltage U_p . There are various methods for measuring the electrical parameters of PMSM as described in [11], [12] and [13]. The resistance R_s is measured using the 4-wire technique at room temperature as the machines temperatures reaches steady state. Most frequently used methods for inductance measurement are no-load and blocked rotor tests for different rotor positions. Even though the blocked rotor test and short-circuit test are complex for performing, the obtained values are more accurate and suitable for high performance systems. No-load (open-circuit)

voltage measurement method is used for determining the back-EMF voltage in the test PMSM when it is driven as a generator. The measured value of basic parameter of PMSM is compared with the data sheet value and presented in Table 3.1. The measured precise machine's parameter will be used to precisely configure VSD.

Table 3.1: The tested PMSM measured parameters.

PMSM parameter	Data sheet value	Measured value
Resistance, R	0.3535 Ω	0.3460 Ω
Inductance, L	4.7 mH	4.5 mH
Back-EMF voltage at 1000 rpm, $U_{p,1000}$	228 V	227.57 V

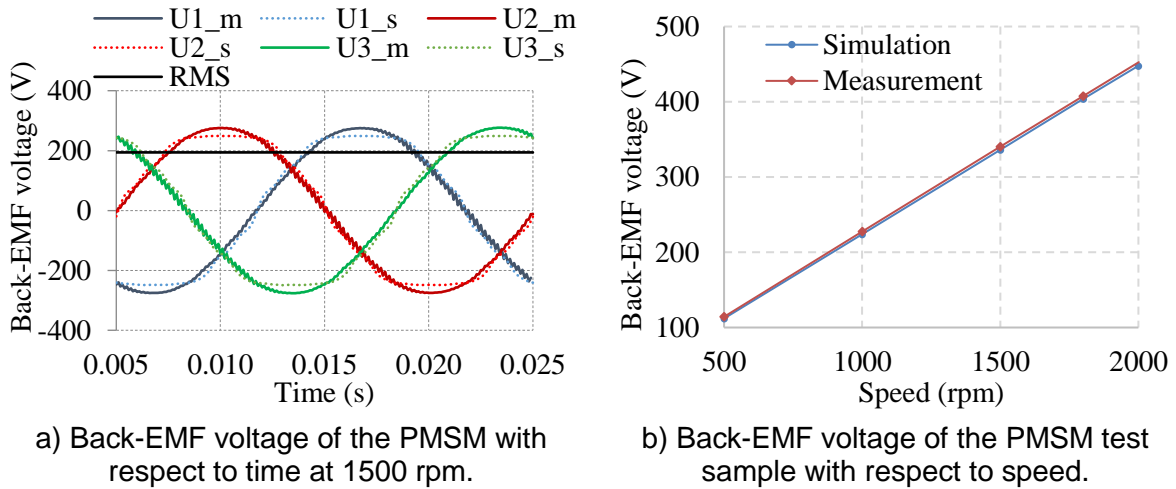


Fig. 3.2. Back-EMF voltage of the PMSM test sample.

The direct efficiency measurement method of PMSM is mentioned and the result is presented in Fig. 3.3. In general, testing and certification of electrical machines with "Ex eb" type of protection does not consist of efficiency measurement. However, the manufacture of the PMSM normally asked for efficiency validation as well. The ratio of measured output power versus input power is used for determining the true efficiency (η) of PMSM in the direct efficiency measurement method. The mechanical output power, $P_{out} = 2\pi \cdot n \cdot M$, is determined by measuring the overall mechanical speed and the mechanical torque of the motor. The electrical input power $P_{in} = 3U \cdot I \cdot \cos \varphi$ of the PMSM is measured using the power analyser WT 3000 manufactured by Yokogawa.

The deviation of the measured value (efficiency) from the true value of measurand is indicated using the measurement uncertainty. The measurement uncertainty helps in defining quality assurance in measurement technology. The calculations of the measurement uncertainty of each measured variable are necessary to certify a corresponding quality for the new measuring test bench for testing of PMSM. The "GUM Workbench" program [14] is used for measurement uncertainty calculations which is discussed.

The mathematical model equation for measuring the effective electrical input power P_{elc} is expressed by the input quantities such as voltage U , current I and power factor $\lambda = \cos \varphi$.

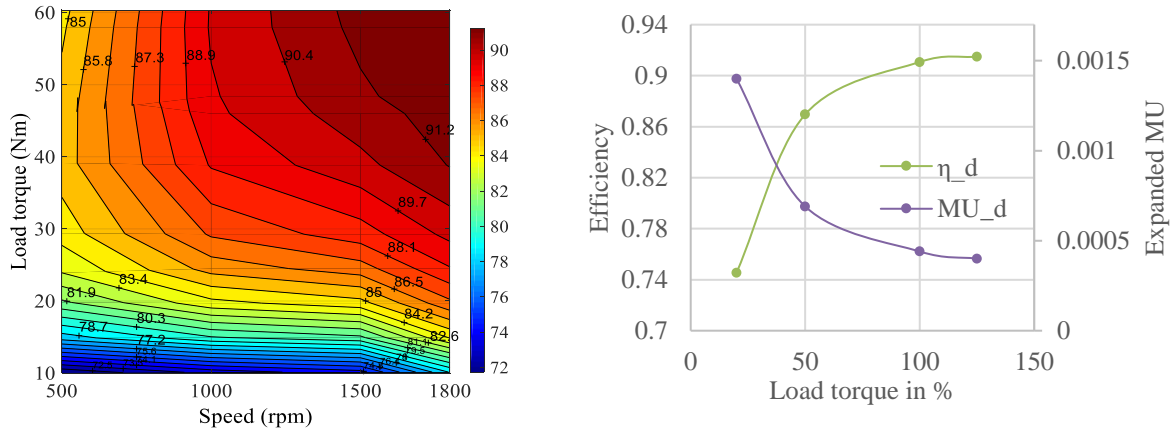
$$y_1 = f(x_1, x_2, \dots, x_N) \text{ i. e. } P_{elc} = f(U, I, \lambda) \quad (3.1)$$

Similarly, mathematical model equation for mechanical output power P_{mech} is expressed by the output quantities such as torque M and speed n .

$$y_2 = f(x_1, x_2, \dots, x_N) \text{ i. e. } P_{mech} = f(n, M) \quad (3.2)$$

Two measurands (electrical input power P_{elc} and mechanical output power P_{mech}) are used to calculate measurement uncertainty while determining the efficiency η_{dir} (direct method) of PMSM.

$$Z = f(y_1, y_2) \text{ i. e. } \eta_{dir} = \frac{P_{out}}{P_{in}} = \frac{P_{mech}}{P_{elc}} = \frac{2\pi \cdot n \cdot M}{3U \cdot I \cdot \lambda} = f(P_{elc}, P_{mech}) \quad (3.3)$$



(a) Efficiency diagram of the test PMSM operation at different speed and different loads.

(b) Efficiency and measurement uncertainty for direct measurement method with varying load for 1500 rpm.

Fig. 3.3. Direct efficiency measurement of the test PMSM with measurement uncertainty.

The measured input quantities with standard measurement uncertainty from the calibration certificate for the rated load and rated speed is shown in the Table 3.2. Using the GUM initially the electrical input power and mechanical output power is calculated which is further used in calculating the combined standard uncertainty of direct efficiency measurement $u_c(Z)$. Then the expanded uncertainty of direct efficiency measurement $U(Z)$ is determined with coverage factor $k = 2$, which corresponds approximately to the coverage probability of 95%. The result is shown in Table 3.3.

Table 3.2: List of input parameters for measurement uncertainty calculation using GUM for direct efficiency determination for rated torque and speed.

Quantity X_i	Value x_i	Standard uncertainty $u_c(x_i)$	Distribution
U	348.6635 V	0.0192 V	Rectangular
I	13.80660 A	0.00146 A	Rectangular
λ	0.988999	0.000140	Rectangular
M	47.80331 Nm	0.00729 Nm	Normal
n	1500.1740 1/min	0.0150 1/min	Normal

Table 3.3: Results of measurement uncertainty calculation using GUM for direct efficiency determination for rated torque and speed.

Quantity Y_j	Value y_j	Expanded uncertainty $U(y_j)$	Coverage factor k_j	Coverage

P_{elc}	8246.1	W	3.1	W	2.00	95% (normal)
P_{mech}	7509.8	W	2.3	W	2.00	95% (normal)
η_{dir}	0.91071		0.000440		2.00	95% (normal)

3.3 Thermal assessment of PMSM

PMSM concerned with Ex machines requires extra attention on its thermal behaviours. Overheating in a PMSM can deficit magnetic properties of permanent magnets resulting in higher current in stator winding. The thermal ageing of insulation and PM yields a significant shortening of the life of the machine. Therefore, determination of temperature distribution in stationary and rotary parts of the PMSM under various operating conditions is extremely important. If the direct measurement of the limiting temperature (i.e. thermal data) throughout the operation cannot be measured, then either calculation or FEM simulation can be used. In the following section wherever possible, the thermal testing results of PMSM with rated load and that with blocked rotor will be presented along with the FEM simulation.

3.3.1. Full load heat run measurement

Thermal steady state behaviour in different parts of the machine is directly measured accurately using the sensors (type T and type K thermocouple). It is possible to conclude that heat run measurement is in steady state condition when the individual measurement sensor temperature rises by less than 1 K/h. It has been demonstrated that the temperature measurement in stator winding and rotor (PM) using direct and indirect method is almost similar. The deviation of the direct and indirect method in measured temperature is ≤ 1.5 K in stator winding and ≤ 4.5 K in rotor temperature. The most challenging and complicated part of the direct rotor temperature measurement has been carried out using telemetry system and has been very successful in determining the PM temperature in real time during rotation state of PMSM. Whereas, the stator winding temperature is measured using thermocouples and 4 wire techniques after the PMSM is stopped.

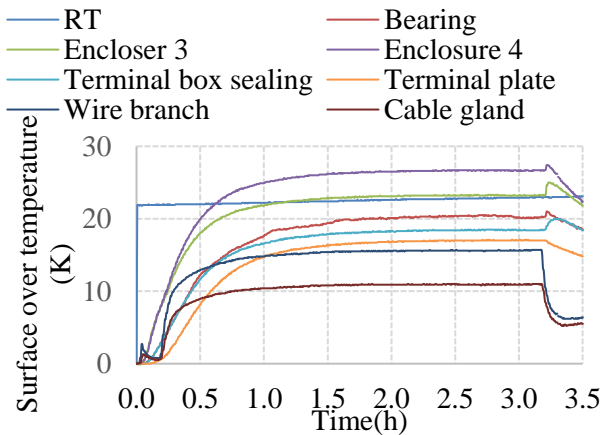


Fig. 3.4. Temperature measurement of the PMSM during the heat run test at rated load and rated speed.

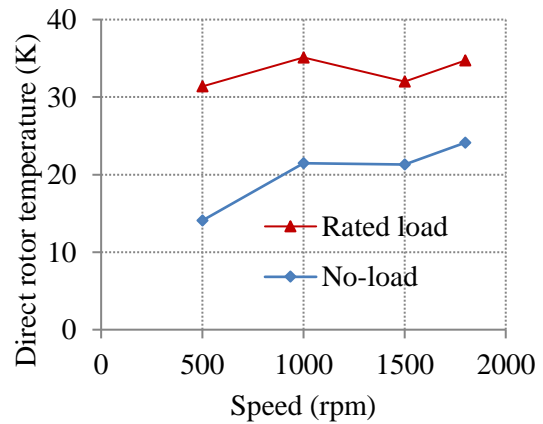
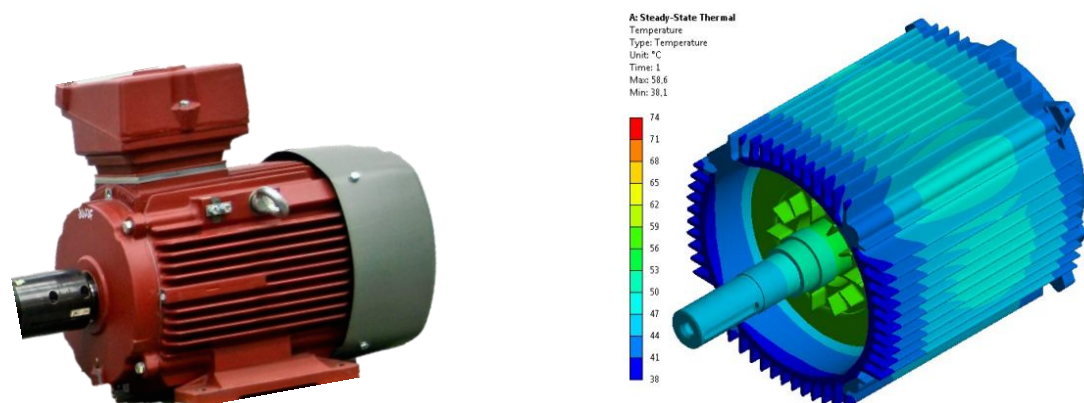


Fig. 3.5. Rotor surface temperatures rise in thermal steady-state at no-load and rated load using telemetry system.

The PMSM FEM model was created and the steady-state simulation results for the rated load and rated speed operation is validated with the measured temperature results. Representing the entire PMSM with a simplified 2D-model (as in Fig. 3.6 (a)) could not yield much accurate results as compared to 3D-model (as in Fig. 3.6 (b)). Table 3.4 shows the comparison of the measured and simulated temperature rise at different positions of the PMSM. The temperature rise is additional temperature to the room (ambient) temperature of 23 °C. Under the same

simulation condition, the 3D simulation produces lower temperatures difference than 2D simulation when compared with the measured value.



(a) Picture of the PMSM used for measurement and simulation.

(b) Resulting temperature distribution of the full 3D simulation model.

Fig. 3.6 Temperature distribution of the PMSM during 3D thermal simulation at rated load and rated speed.

Table 3.4: Comparison of simulated vs measured temperature rise of PMSM at rated load and rated speed.

Location	Measured temperature rise	Simulated temperature rise
	θ_{measured} (K)	$\theta_{\text{3D-simulation}}$ (K)
PM	32.0	34.4
Stator windings	33.1	35.6
Frame	26.7	25.6

The thermal measurement in full load and rated speed have been able to compare and validate with the 2D and 3D FEM thermal simulation. The comparison shows the good agreement between the measured and the FEM 3D simulation. Especially with the 3D simulation at the rated operation, the temperature rise agreement is within $\sim 7.5\%$ in PM, $\sim 7.6\%$ in stator winding and $\sim 4.1\%$ in frame (i.e. enclose 4 in the thermal measurement). The FEM 3D thermal simulation is based on accurate thermal heat sources, heat transfer elements and heat storage elements in PMSM, therefore the simulation provides a reasonably better analysis compared to the FEM 2D thermal simulation where no overhang winding thermal behaviour is considered.

3.3.2. Overload measurement including thermal protection using inbuilt sensors

The PMSM fed with variable speed drive (VSD) is operated with overload conditions the surface temperatures can be above the permitted temperature. In this scenario the available protection system should activate and stop the operation of the PMSM to avoid the damage of the machines. The functionality test of the available temperature sensors (PTC) in stator winding as shown in Fig. 3.7 must be experimentally tested during overload condition of the machines. However, there is no any specific test method that helps to verify the temperature limit of stator and rotor of PMSM. Therefore, in this section, the temperature measurement of the VSD fed PMSM in over load condition is presented focusing on the temperature limiting functionality test during over-temperature operation.

The PTC thermistors tripped when the winding over temperature $\Delta\theta_{WOT}$ is within the following limit:

$$\theta_{Amb} + \Delta\theta_{Nom} - 5K < \Delta\theta_{WOT} < \theta_{Amb} + \Delta\theta_{Nom} + 20K \quad (3.4)$$

where, with θ_{Amb} is the maximum ambient temperature in °C and $\Delta\theta_{Nom}$ is the winding overtemperature at nominal or rated operation in K. The selection of the PTC from equation (3.4) provides the range of the operating margin of 25 K. This margin helps in preventing malfunction of the PTC and approximately trigger in higher temperature during the overload condition.

The overall measurement results for different PTC thermistor operations are summarized in Table 3.5. To illustrate the measurement results, a measurement method with gradual increase in load torque at rated speed is presented for 80 °C PTC thermistors in Fig. 3.8. In the Table 3.5 the winding resistance is determined using the extrapolated cooling curve of winding resistance at zero second after the PTC triggering signal is on. Whereas, the PM temperature is directly measured using the telemetry system.

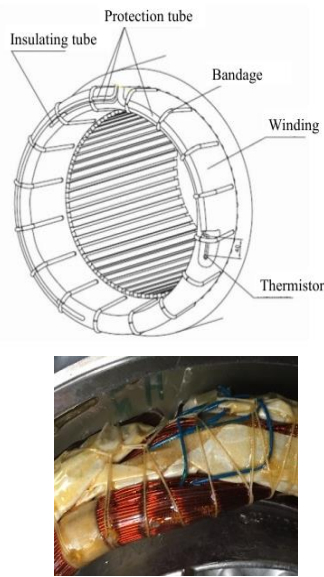


Fig. 3.7. Thermistors in the winding according to IEC 60079-7.

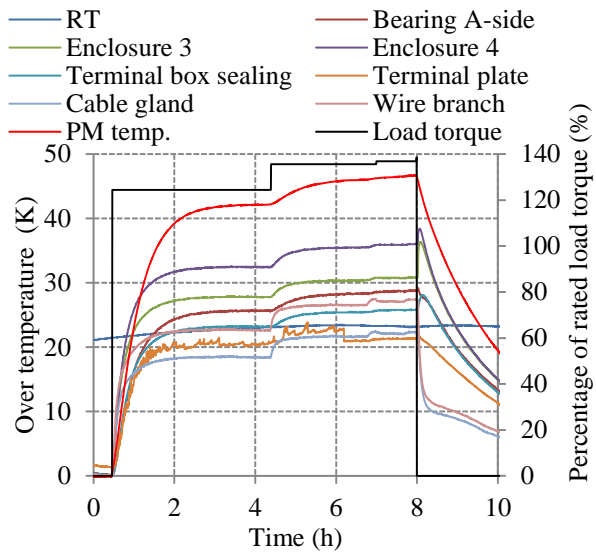


Fig. 3.8. Surface over temperature w.r.t. room temperature of the PMSM at rated speed during overload test.

Table 3.5: PTC triggering measurement results summarized with respect to winding and ambient temperature.

Speed	Stator winding and PM temperature when the PTC 80 °C is triggered		
	$\Delta\theta_w$ (K)	$\Delta\theta_{PM}$ (K)	RT (°C)
150	58.3	43.1	24.4
500	60.2	45.9	23.8
1000	61.8	47.4	23.4
1500	63.1	46.7	23.2
1800	64.1	45.6	23.8

The test results of PTC triggered assure the scenario in which the PTC is activated and provide the thermal protection of the VSD fed PMSM. The test method is simply adopted from ASM overload test and is still valid for the PMSM. Whereas for the selection of the PTC thermistors sensor the manufacturer need to pay attention on the operating temperature of the PM that are used in manufacturing the rotor of the machine and its demagnetization phenomenon. The online measured rotor temperature of the PMSM is generally small compared to calculated stator temperature as summarized in Table 3.5. Therefore, if the online rotor temperature

measurement system is not available then indirect temperature measurement of the rotor temperature can be done.

The PMSM with protection “eb”, directly fed with VSD supply shall be equipped with PTC thermistor sensor to protect the thermal heating of the winding. The experimental confirmation of the PTC thermistors sensor functionality test is required before issuing the certification of PMSM in hazardous environment.

4 Possible failure and demagnetization analysis of PMSM using FEM simulation

In general, the stator winding of electrical machines due to winding insulation failure is one of the many elements which could lead to malfunctioning of the machines. The turn-to-turn faults or “stator turn fault” is more common in electrical machines caused by insulation failures in several turns of a stator coil within one phase. Turn-to-turn short circuits, however, cause very small effects at first, but will then evolve and possibly inflict catastrophic damage [15] and [16].

The abnormal conditions such as three phase faults is investigated based on finite element method (FEM) simulation in commercially available Opera 2D RM software. Three different simulation sections are compared in one RM simulation to study demagnetization of the PM. In the first section, the PMSM runs as open circuit without the stator currents. This results in the back-EMF voltage and magnetic flux density of the PM with small impact of external circuits on the results. The result is similar to open circuit test in normal operation since the internal resistance is normally much lower than the added external resistance. In the second section, the three-phase short circuit is generated in the stator winding. The final and third section is the clearing of the faults and considering the open circuit simulation.

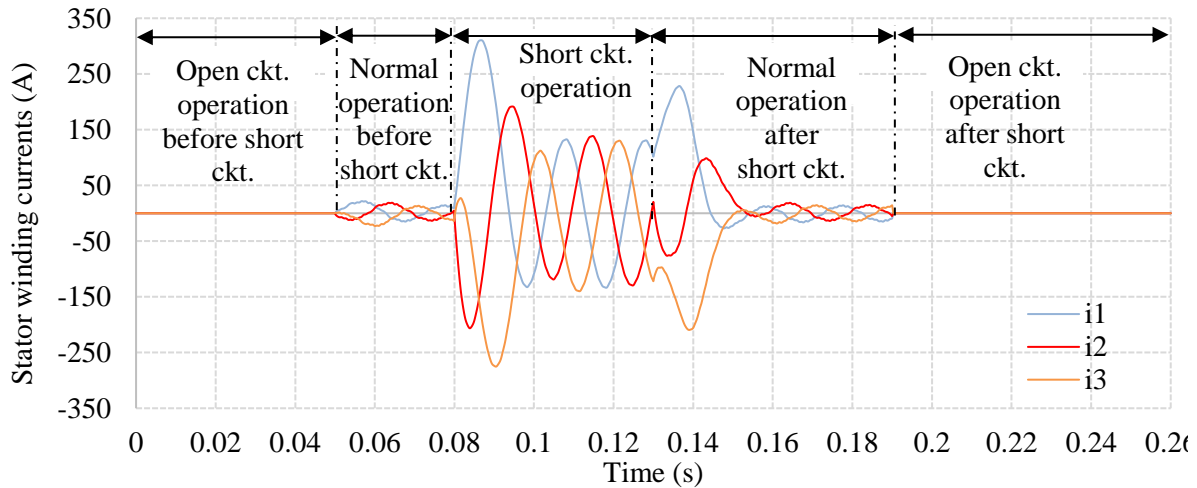
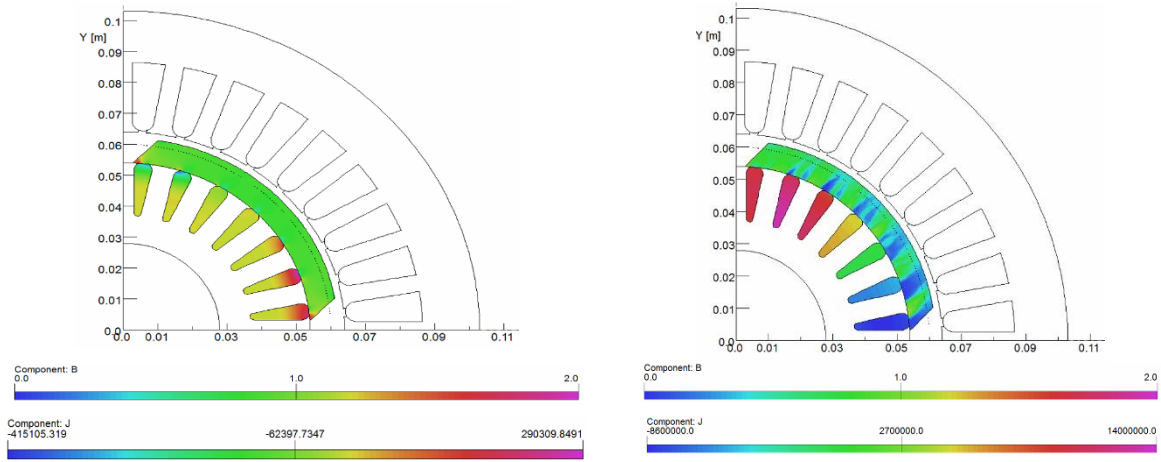


Fig. 4.1. Stator winding currents during normal operation (0.05-0.08 s), short circuit (ckt.) operation (0.08-0.14 s) and re-synchronization currents (0.14-0.19 s) after short circuit is removed from PMSM.

The percentage change of back-EMF voltage after the faults clearance explain the damage caused in the PM due to three-phase faults. The demagnetization index D_M is used to express the percentage of demagnetization which is calculated as:

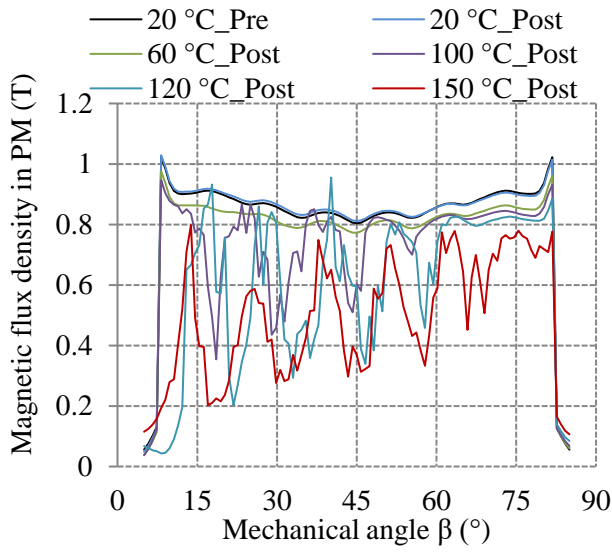
$$D_M = 1 - \frac{\iiint |\bar{B}|_{t=t_4} dV}{\iiint |\bar{B}|_{t=t_1} dV} \% \quad (4.1)$$

Where $t = t_1 = 0.04 \text{ s}$ is the reference time where the PM is healthy and considered as the initial state of the magnets, $t = t_4 = 0.2 \text{ s}$ is the time after which all the transient current effect due to failure is decayed to zero and \iiint is volume integral of PM.

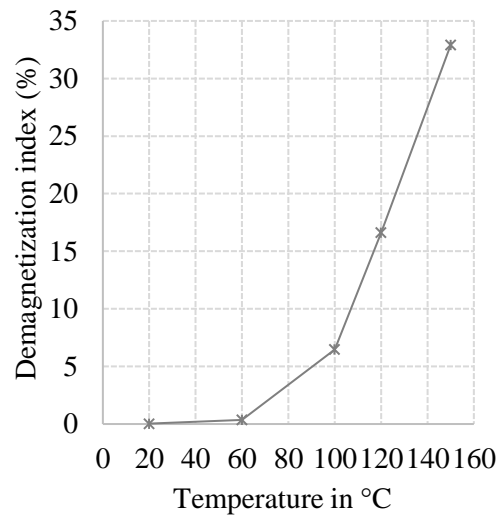


(a) Magnetic flux density distribution in a PM and current density in bars of squirrel cage rotor at 20 °C and $t = t_1 = 0.04 \text{ s}$ before fault.

(b) Magnetic flux density in PM and current density in bars of squirrel cage rotor at $t = t_4 = 0.2 \text{ s}$ and 150 °C after three-phase short circuit.



(c) Comparison of the magnetic flux density in 2 mm below the surface of PM at different temperature.



(d) Demagnetization index in % representing the decrease in B w.r.t. different operating temperature before and after three phase short circuit at the rated speed of 1500 rpm.

Fig. 4.2. Magnetic flux density distribution in a PM after three-phase short circuit scenario to study demagnetization of PM.

In order to determine the demagnetization of PM, two methods are proposed, namely: Back-EMF voltage value and magnetic flux density distribution in the PM after faults. Open circuit simulation is performed before and after faults and the comparison is presented. One of the big advantages of these approaches for demagnetization with the help of simulation is that there is no risk of damaging the test samples of PMSM. However, proper materials parameters for the simulation must be defined by the user. A key limitation of FEM based demagnetization study presented in this chapter is that it does not address the experimental result. Clearly,

further research on reliable experimental method will be needed to validate the FEM results in order to diagnose the demagnetization of a PMSM.

Table 4.1: Summary of irreversible demagnetization of PM after three phase faults conditions.

Abnormal conditions	Back-EMF value after faults (%)			Demagnetization index after faults at 120 °C (%)		
	20 °C	100 °C	150 °C	20 °C	100 °C	150 °C
Three phase faults	0.03	8.66	41.526	0.04	6.47	32.91

In this section, the irreversible demagnetization diagnosis method based on Opera 2D/RM FEM simulation during abnormal conditions is analysed and presented for PMSM. The overall simulation results are focused on the irreversible demagnetization of PM after faults occurred in the PMSM. The simulation method is an effective way to study demagnetization effect of the machines while measurement-based study regarding failure of PMSM is cost ineffective and tedious way to analyse the performance of the machines.

5 Summary

In this paper, the energy efficient PMSM is experimentally investigated that are planned to be used in hazardous areas as the “Increased Safety” type of ignition protection classification. This work has underlined the importance of the magnetic properties of the magnetic materials of PMSM and satisfactorily presented the results that could be applied to study and understand the PMSM in higher temperature and higher frequency operation. The simple methodology for type test and certification of PMSM is presented to provide the basic guidance for testing and certification of PMSM with VSD that are planned to be used in hazardous areas. The proposed methodology can be readily used in practice mainly by motor manufacturer (construction, design, repair, testing and sales), by the user (especially in the mining, chemical and petrochemical industries), by the responsible inspection authorities (approval authorities, work inspectors, trade associations and the technical inspection organization), by the recognized experts and by testing labs in Germany and abroad.

6 References

- [1] IEC 60079-10-1, *Explosive atmospheres - Part 10-1: Classification of areas - Explosive gas atmospheres*, 2nd ed. .
- [2] IEC 60079-0, *Explosive atmospheres - Part 0: Equipment - General requirements*, 6th ed. 2011.
- [3] IEC 60079-7, *Explosive atmospheres – Part 7: Equipment protection by increased safety “e,”* 5th ed. 2015.
- [4] N. Yogal, C. Lehrmann, and M. Henke, “Investigations on permanent magnetic materials to be used in explosion-protected permanent magnet synchronous machines,” in *Proceedings of the International Conference on Power Electronics and Drive Systems*, 2015, vol. 2015–August.
- [5] N. Yogal, C. Lehrmann, M. Henke, and X. Liu, “How to measure the demagnetization of permanent magnet synchronous machines used in explosive environments,” in *2017 IEEE International Electric Machines and Drives Conference, IEMDC 2017*, 2017.
- [6] A. Binder, *Elektrische Maschinen und Antriebe: Grundlagen, Betriebsverhalten*. Springer, 2012.
- [7] S. Tumanski, *Handbook of Magnetic measurements*. Florida, US: CRC Press, 2011.
- [8] IEC 60404-6, *Methods of measurement of the magnetic properties of magnetically soft*

- metallic and powder materials at frequencies in the range of 20 Hz to 200 kHz by the use of ring specimens*, 2nd ed. 2003.
- [9] C. Lehrmann, "Über ein Zulassungsverfahren für explosionsgeschützte, umrichter gespeiste Käfigläufer der Zündschutzart „Erhöhte Sicherheit“,“ Ph.D. dissertation, Gottfried Wilhelm Leibniz Universität Hannover, Hannover, Deutschland, 2006.
- [10] R. McElveen, B. Martin, E. Massey, and D. Stelzner, "Applying permanent magnet motors in an ex environment," in *Industry Applications Society 60th Annual Petroleum and Chemical Industry Conference*, 2013, pp. 1–7.
- [11] P. Vas, *Parameter estimation, condition monitoring, and diagnosis of electrical machines*. Clarendon Press, 1993.
- [12] W. L. Soong, "Inductance Measurements for Synchronous Machines," *Power Eng. Brief. Note Ser.*, 2008.
- [13] M. Štulrajter and M. Mušák, "Unconventional methods for PM Synchronous Motor parameters investigation," *2012 ELEKTRO*. pp. 260–265, 2012.
- [14] Metrodata GmbH, "GUM Workbench User Manual for Version 1.4 and 2.4," 2010. [Online]. Available: http://www.metrodata.de/downloads/GUM_Workbench_User_Manual.pdf. [Accessed: 25-Aug-2017].
- [15] S. Mortazavizadeh, "A Review on Condition Monitoring and Diagnostic Techniques of Rotating Electrical Machines," *Phys. Sci. Int. J.*, vol. 4, no. 3, pp. 310–338, Jan. 2014.
- [16] Y. Gritli, "Diagnosis and Fault Detection in Electrical Machines and Drives based on Advanced Signal Processing Techniques," Ph.D. dissertation, University of Bologna, Bologna, Italy, 2014.